Nuclear Instruments and Methods 176 (1980) 151–157

Part III. Cylindrical chambers, vertex detectors

THE LARGE CYLINDRICAL DRIFT CHAMBER OF TASSO

H. BOERNER, H.M. FISCHER, H. HARTMANN, B. LÖHR *, M. WOLLSTADT
Physikalisches Institut der Universität, Bonn, Germany ***

D.G. CASSEL **, U. KÖTZ, H. KOWALSKI, B.H. WIIK
Deutsches Elektronen-Synchrotron DESY, Hamburg, Germany

R. FOHRMANN and P. SCHMÜSER
II. Institut für Experimentalphysik der Universität, Hamburg, Germany ***

We have built and operated a large cylindrical drift chamber for the TASSO experiment at the DESY storage ring, PETRA. The chamber has a length of 3.5 m, a diameter of 2.5 m, and a total of 2340 drift cells. The cells are arranged in 15 concentric layers such that tracks can be reconstructed in three dimensions. A spatial resolution of 220 μm has been achieved for tracks of normal incidence on the drift cells.

1. Introduction

The cylindrical drift chamber described here is the main part of the TASSO [1] experiment (fig. 1) at the DESY storage ring, PETRA. It is mounted inside a solenoidal coil providing a uniform magnetic field of 0.5 T parallel to the beam axis.

Particles originating from the interaction region traverse the beam pipe and pass through a segmented scintillation counter. They then enter the tracking part of the inner detector consisting of a four layer proportional chamber and the drift chamber. 48 time of flight counters form a cylindrical shell around the drift chamber.

The drift chamber is designed to measure the trajectories of charged particles in the full solid angle, to provide a fast trigger and to reconstruct tracks in three dimensions. The momentum of the particle is determined from the curvature of the track in the magnetic field.

Since typical hadronic events at PETRA energies were expected to have high charged multiplicities with the particles emitted in narrow jets [2], the chamber was designed to resolve closely spaced tracks.

* Now at SLAC, Stanford, U.S.A.
** On leave from Cornell University, Ithaca, U.S.A.
*** Supported by the Bundesministerium für Forschung und Technologie.

2. Design

The body of the chamber consists of two circular endplates, an inner tube, and an outer shell. The dimensions are given in fig. 2. Each endplate is a solid piece of aluminium, 35 mm thick, with a diameter of 2560 mm. Each has 9360 holes for the wire feedthroughs. The endplates are held apart by the inner tube and the outer shell which support the tension of the wires of 22.5 kN. The inner tube is made of 5 mm fibreglass-epoxy to minimize the amount of material between the interaction point and the chamber. The outer shell consists of 6 mm thick aluminium plates which form the surface of a cylinder.

The chamber has 2340 identical drift cells with the simple structure shown in fig. 3 [3]. The fundamental pattern consists of only four wires, a triplet of potential wires and the sense wire. This is repeated around the circumference of a circle, yielding drift cells separated by the potential wires. In the radial direction the cells are open. This configuration has the minimal number of potential wires, but it precludes fieldshaping to compensate for the influence of the magnetic field. All cells have a height of 12 mm and the distance between a sense wire and the nearest potential wires is 16 mm measured along the arc. The cells are arranged in 15 equally spaced concentric layers. The radii range from 367 mm for the innermost layer to 1222 mm for the outer one, with 61.1 mm between layers. Nine of the layers have the sense wires parallel

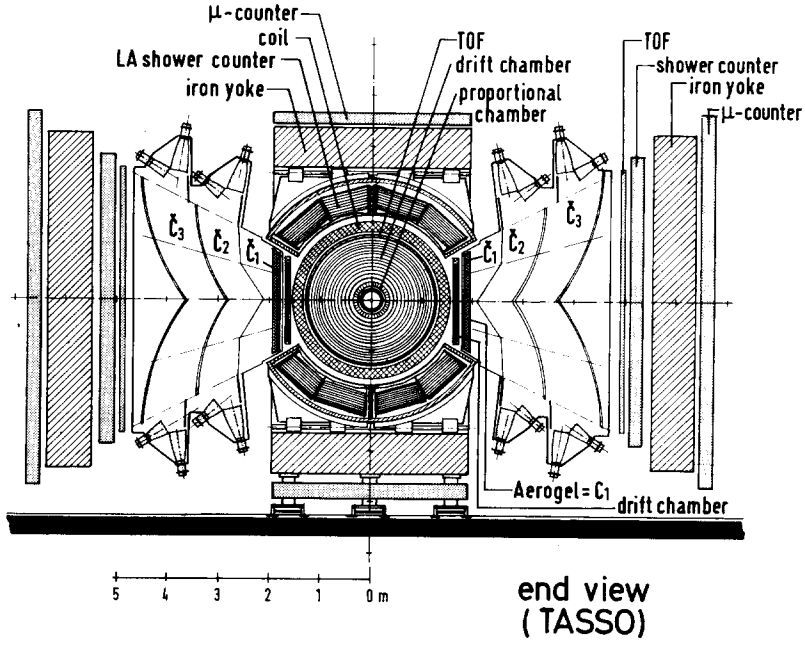

Fig. 1. The TASSO detector viewed along the beam.

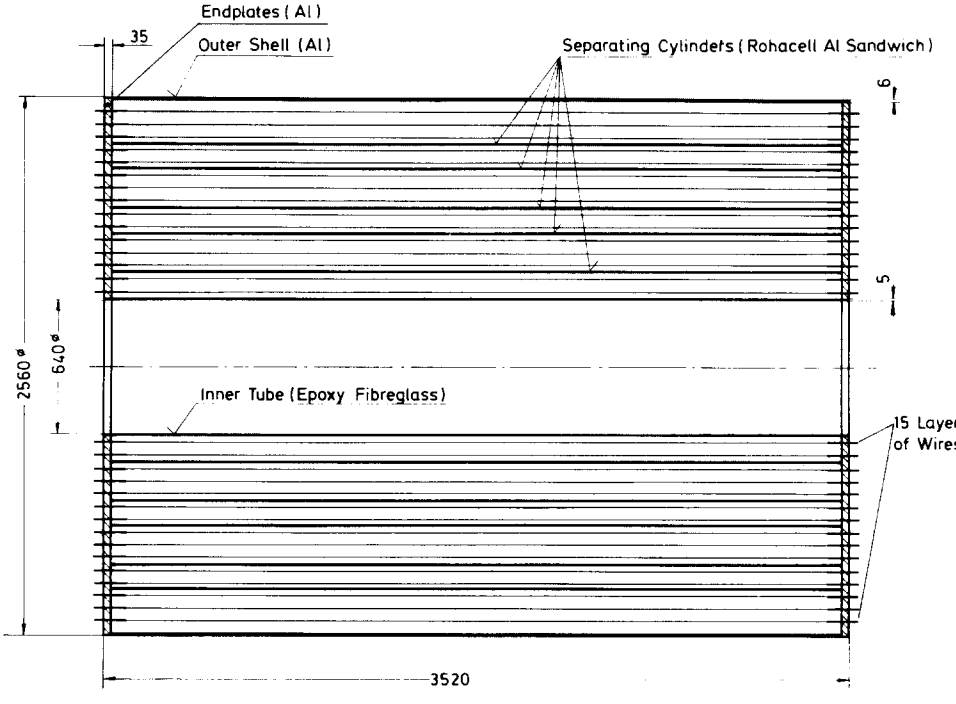

Fig. 2. Schematic drawing of the drift chamber (dimensions in mm).

TABLE 1
Data on the cell layers.

Layer	No. of drift cells	Radius (mm)	Stereo angle
1	72	367	0°
2	84	428	+3.36°
Separating cylinder: 4 mm Rohacell, 2 × 10 μm Al			
3	96	489	0°
4	108	550	−3.37°
5	120	611	0°
Sep. cyl.: 4 mm Rohacell, 2 × 10 μm Al			
6	132	672	0°
7	144	733	+3.94°
Sep. cyl.: 4 mm Rohacell, 2 × 10 μm Al			
8	156	795	0°
9	168	856	−4.50°
10	180	917	0°
Sep. cyl.: 10 mm Rohacell, 2 × (8 μm Al; 10 μm polyester)			
11	192	978	0°
12	204	1039	+4.50°
Sep. cyl.: 10 mm Rohacell, 2 × (8 μm Al, 10 μm polyester)			
13	216	1100	0°
14	228	1161	−4.51°
15	240	1222	0°

to the beam axis providing coordinates in a plane perpendicular to this axis. The wires of the remaining six layers are strung at a small angle with respect to the beam axis. The wires of these stereo layers follow the generating lines of rotational hyperboloids. Longitudinal coordinates are determined with the help of these stereo layers.

Some relevant data about the 15 layers are summarized in table 1. The cell pattern has a 12-fold symmetry, it is repeated every 30°. Four of the 0° layers are rotated by half a cell size, so that the sense

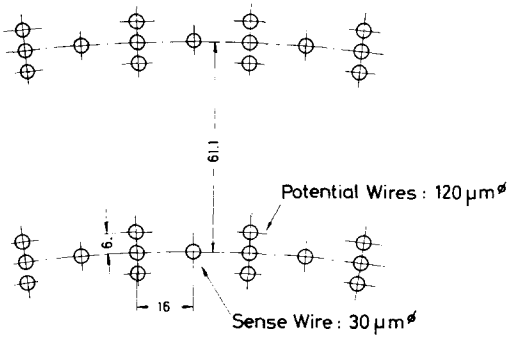

Fig. 3. Drift cell geometry.

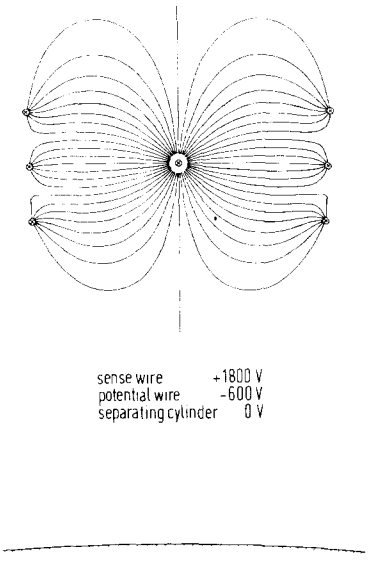

Fig. 4. Electric field lines in one drift cell. Crosses mark the positions of the wires. The separating cylinder is indicated below.

wires do not line up at the boundaries of the 30° sectors. Five separating cylinders divide the chamber into 6 compartments. This physical separation improves the operational security because the damage caused by a broken wire will be confined to one compartment. The cylinders have a conductive surface which is at ground potential. To minimize field distortions in the drift cells, the potential wires are at a negative voltage and the sense wires at a positive one in a ratio of 1 : 3. The same potentials are used in all layers.

The electric field resulting from the cell geometry, the wire diameters, and the position of a separating cylinder is shown in fig. 4.

3. Construction

3.1. Mechanics

The assembly of the chamber was carried out in a clean room. At first the endplates were fastened to the inner pipe and aligned.

To allow free access to the chamber volume for the duration of the assembly, reinforcing bars were substituted for the outer shell.

We used 30 μm gold plated tungsten wire [4] for

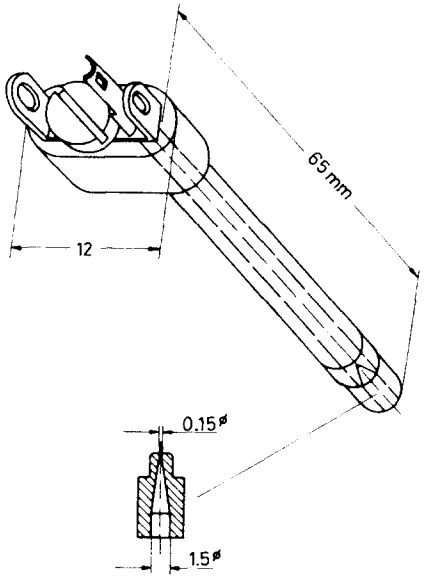

Fig. 5. Wire feedthrough.

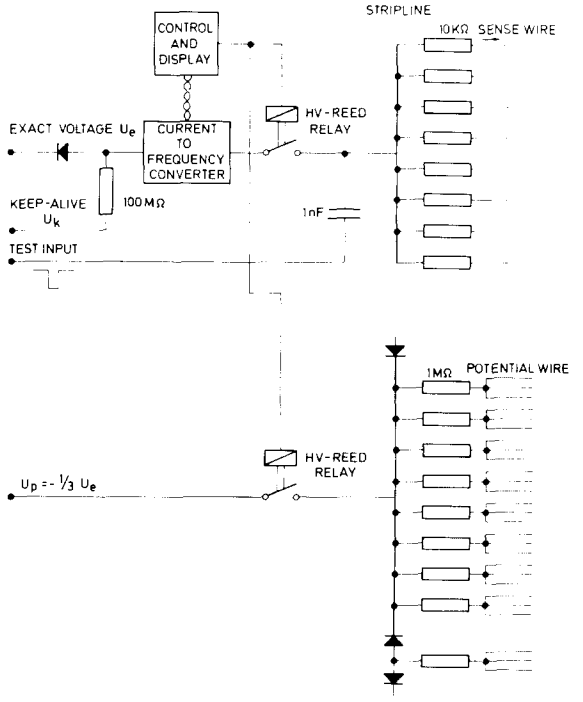

Fig. 6. Scheme of the high voltage system.

the sense wires and 120 μm gold plated molybdenium wire [5] for the potential wires. A 30 μm sense wire was chosen instead of the often used 20 μm wire because the thinner wire breaks more easily and prohibits the use of high electric fields in the cell. The molybdenium wire was chosen because it had the smoothest surface and does not curl after breaking.

The feedthrough shown in fig. 5 is used for both sense and potential wires. It consists of two parts, namely the actual feedthrough with a support for a soldering tag on the outer end and a small tip with a 150 μm hole. The material used is extruded Hostaform C [6]. The center of the hole deviates from the axis of the feedthrough by less than 50 μm. The positions of the holes in the endplates are accurate to better than 100 μm. The wires were strung by hand and loaded with a force of 0.8 N for the sense wires and 3 N for the potential wires. Then they were soldered to the soldering tag at the outer end of the feedthrough. We used a solder alloy with a low melting point (145°C) [7] to reduce the dissolving of the gold plating. In addition the wires were glued to the tag.

The tension of each wire was checked by measuring its sag with an optical level after a small weight was hung from the wire. As each layer was completed, high voltage was applied to the sense wires and the current drawn was measured. If a wire had a current in excess of 2 nA, it was cleaned with a soft brush and pure ethanol. This cure failed in very few cases, where the wires had to be replaced.

The separating cylinders are made of hot-moulded polyacrylic foam [8], sandwiched between aluminium or aluminium clad polyester foils (table 1). This results in a low mass structure (<1% of a radiation length) which is nevertheless quite rigid.

3.2. The high voltage system

The high voltage distribution and safety system is shown in fig. 6. To ensure safe operation, the chamber is divided into 90 separate groups. Each one is equipped with its own current limiting device. The high segmentation of the chamber enables us to keep the current limit per group as low as 10 μA. Both a passive and an active "fuse" are used, each one acts on the voltage supply for the sense wires.

The passive "fuse" is a diode switch with a characteristic shown in fig. 7 [9]. The reaction time is on the order of 10 μs. In addition we use a current-to-frequency converter [10]; it is designed to operate without external power supplies. If the frequency exceeds a certain limit, both sense and potential wires of the corresponding group are disconnected from the hv power supply. The limit for this "fuse" is set

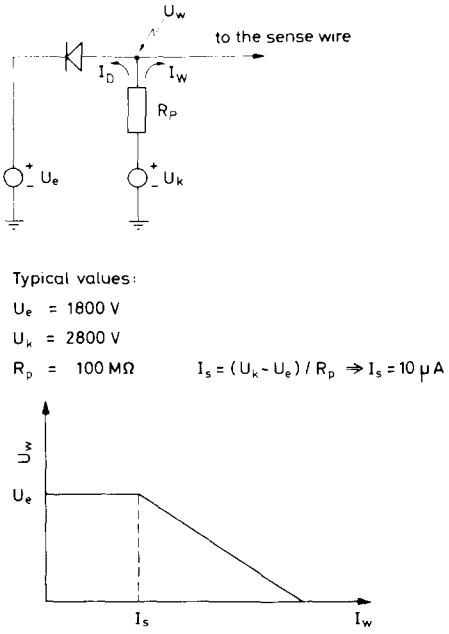

Fig. 7. The diode switch and its characteristic.

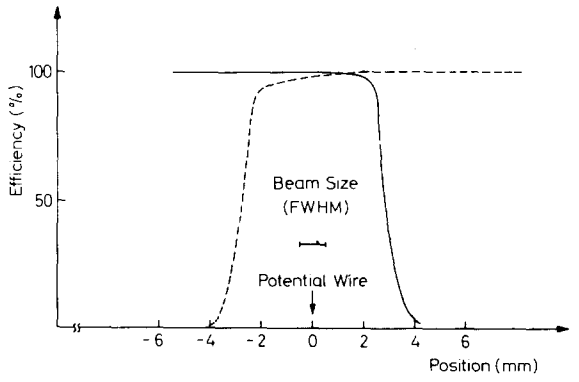

Fig. 9. Efficiency in two neighbouring cells, measured in a small test chamber with a magnetic field of 0.5 T parallel to the wires. The cells were scanned with a narrow beam. The effect of crosstalk is clearly seen.

slightly lower than for the diode switch to produce an alarm if excess current is drawn. Should a wire break in spite of these protective measures, the affected group can be disconnected and operation can be resumed. This safety system has worked very reliably. Several times the beams were accidentally dumped near the experiment resulting in an emergency switch off for nearly all 90 groups, but no damage to the chamber was observed.

3.3. Electronics

Fig. 8 shows the scheme of the readout system. The signals are coupled out on one endflange since only drift-time information is used. The sense wires are connected to amplifier-discriminators [11] via coupling capacitors and 4 m coaxial cables. The pulses are shaped and then sent via twisted pair cables to an active latch and fanout which splits the signals and feeds them to the fast trigger logic and the TDCs. We use a commercially available TDC system [12] with single hit capability.

3.4. Gas supply

The chamber volume is uniformly flushed by means of a manifold system, which distributes the gas evenly to the six compartments. The flow rate is adjusted to 1.2 m^3/h, and the gas is not recycled. We operate the chamber with a 90 : 10 mixture of argon–methane. The gas is mixed at the experiment, using the boiloff from a liquid argon tank, to which methane of 99.995 grade purity is added. Methane has the advantage of being comparatively inexpensive at this level of purity, but we have to accept rather large nonuniformities in the space drift-time relation when operating in a magnetic field. Another disadvantage is the tendency for cross talk between neigh-

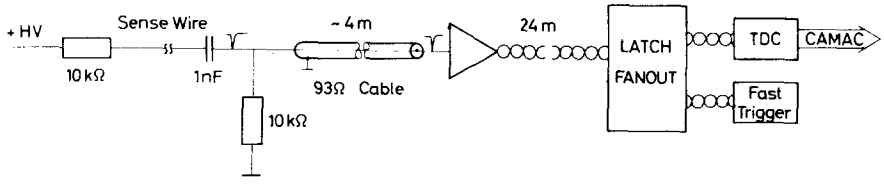

Fig. 8. Scheme of the readout electronics.

bouring cells, as shown in fig. 9. The nonlinearities are accounted for in the track fitting procedure and the cross talk only slightly complicates the track finding procedure and the measurement of the space drift-time relation.

4. Operation

The chamber has worked very reliably since it was installed in late 1978. So far no single wire has broken and there has been no sign of glow discharges.

Fig. 10 shows the hit pattern of a hadronic event together with the reconstructed tracks. For sake of clarity only the hits in the 0° layers are shown. The efficiency was measured using cosmic ray events. Fig. 11 gives the plateau curves taken at 0 and 0.5 T. These measurements were made with the threshold of the amplifier-discriminators set to 0.5 mV. Based on the plateau curve for a field strength of 0.5 T, the operating voltage was set to 2470 V. The observed plateau efficiency ($\geqslant$98%) includes an electronic inefficiency of 0.5%, so the chamber efficiency is $\geqslant$98.5%. The efficiency is not reduced by the background caused by the stored beams in PETRA.

The space drift-time relations were determined by

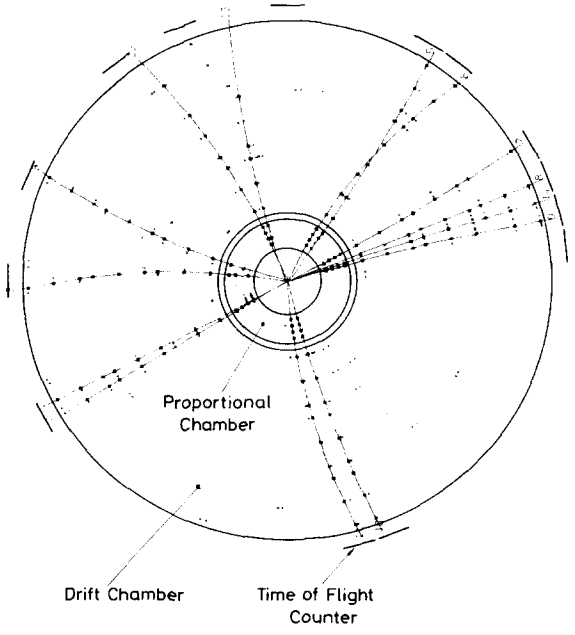

Fig. 10. A hadronic event at 35.8 GeV c.m. energy. Only the hits in the 0° layers are shown. No background hits are removed.

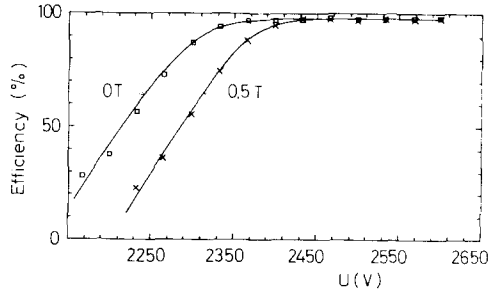

Fig. 11. Plateau curves taken at field strengths of 0 and 0.5 T The efficiency has not been corrected for electronic failures.

an iterative, selfconsistent method using the tracks of approximately 25 000 cosmic ray events. First the tracks are fitted with an approximate space drift-time relation. Then the residuals, i.e. the difference between the fitted track and the position associated with the drift time, are calculated and accumulated. The mean residuals are then used to correct the previous space drift-time relation. The fitting procedure is then repeated until further corrections become negligible. The procedure takes 5–7 passes.

Fig. 12 shows the space drift-time relations obtained by this method. Up to a distance of 6 mm from the sense wire the relation is nearly independent of the angle of incidence. At larger distances they depend on both the magnitude and the sign of the entrance angle. The greater part of this effect, apart from trivial geometrical reasons, is due to the deflection of drifting electrons by the magnetic field. This leads to a variation in the length of the drift-paths and correspondingly to a change in the drift-time.

This effect is rather large; a measured drift-time of 500 ns corresponds to distances from the wire between ~11 mm and ~15 mm depending on

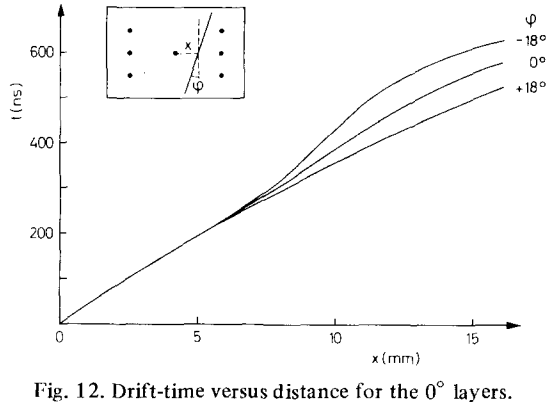

Fig. 12. Drift-time versus distance for the 0° layers.

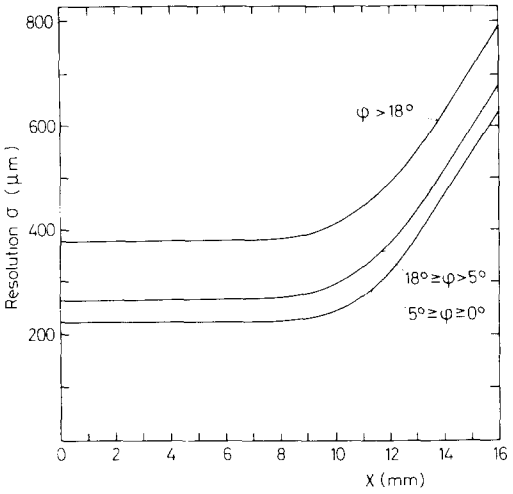

Fig. 13. The spatial resolution achieved, measured with Bhabha events and hadronic events. The resolution for 0° layers is plotted versus the position in the cell for various entrance angles.

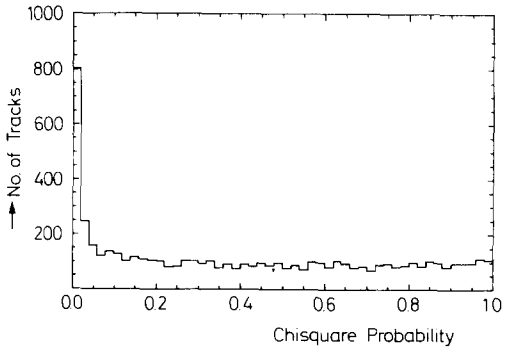

Fig. 14. Chi-square probability plot using the tracks of Bhabha events.

whether the entrance angle is +18° or −18°. Using these space drift-time relations we have determined the spatial resolution of the chamber. One of the cells on a track was left out of the fit and the difference between the position assumed by the fit and the measured position was plotted. The width of the curve obtained is a combination of the resolutions of the chamber, the accompanying electronics, the drift-time corrections and the fit. The results with the error in the fit unfolded are shown in fig. 13.

The curves are approximate parametrisations of the data points. For normal incidence we obtain a resolution of 220 μm. The resolution is constant for more than 2/3 of the cell width. It deteriorates near the potential wires. In this region the space drift-time relations are not yet precisely known. Using the resolutions as weights in a circle fit to the tracks we obtain consistent results for 95% of all tracks. This is shown by the χ^2 probability plot (fig. 14), where 95% of the entries give a flat distribution indicating a gaussian error of the assumed width. 5% of the tracks produce the peak at low probabilities; this is probably due to incorrectly assigned hits giving rise to large non gaussian errors.

At present we have achieved a momentum resolution of $\sigma_p/p = 0.02p$ (p in GeV/c) determined from a measurement of muon pair production using both 0-degree and stereo chambers but not the interaction point in the fit.

Further efforts will concentrate on an improved determination of the space drift-time relations. In addition, some small corrections to the measured drift-time which so far have been neglected will be included. Among these are errors in the wire positions, the wire sag, and nonuniformities of the magnetic field.

The construction of the drift chamber on the tight time scale was a considerable task and would not have been accomplished without the tremendous efforts of the engineers and technicians of the collaborating institutes. In particular we thank D. Brauer, G. Krohn, H.J. Schirrmacher, W. Sieburg, T. Stoetzer and W. Winkelmann. We are indebted to Dr. M. Tonutti for many helpful discussions in the design stage. We thank Dr. E. Hilger for stimulating remarks on this paper. The many contributions of the TASSO collaboration especially in data handling and processing are highly appreciated.

References

[1] The TASSO collaboration: see, for example, R. Brandelik et al., Phys. Lett. 83B (1979) 261.
[2] G. Hanson et al., Phys. Rev. Lett. 35 (1975) 1609.
[3] This cell structure was first proposed by D. Hartill (Cornell University).
[4] Lumalampan A.B. Stockholm, wire type 861/20, contains 2% Re for higher breaking point.
[5] Thyssen Edelstahlwerk AG–Sondermetalle Stuttgart, wire quality G (half hard).
[6] Tradename of Hoechst AG, Frankfurt.
[7] Kueppers Metallwerk, Bonn, alloy Sn Pb Cd 50/32/18.
[8] Rohacell, tradename of Roehm GmbH, Darmstadt, density 30 kg/m^3.
[9] L. Baksay et al., Nucl. Instr. and Meth. 133 (1976) 219; C.R. Kerns, IEEE Trans. Nucl. Sci. NS-24 (1977) 205.
[10] R. Hammarstroem (CERN), private communication.
[11] Modified version of CERN design 4242.
[12] Le Croy Research Systems Corp., modell 2770 A, 2.6 ns time resolution.